SUPPORTING ONLINE MATERIAL

Retrograde synaptic inhibition is mediated by α-Neurexin binding to the α2δ subunits of N-type calcium channels

Authors: Xia-Jing Tong[1,2], E. Javier Lopez-Soto[4], Lei Li[5], Haowen Liu[5], Daniel Nedelcu[1,2], Diane Lipscombe[4], Zhitao Hu[5], and Joshua M. Kaplan[1,2,3,*]

Affiliations:

[1]Department of Molecular Biology, Massachusetts General Hospital, Boston, MA 02114, USA

[2]Department of Neurobiology, Harvard Medical School, Boston, MA 02115, USA

[3]Program in Neuroscience, Harvard Medical School

[4]Department of Neuroscience and Brown Institute for Brain Science, Brown University, Providence, RI 02912

[5]Clem Jones Centre for Ageing Dementia Research, Queensland Brain Institute, The University of Queensland, Brisbane, Australia

[*]Correspondence to: kaplan@molbio.mgh.harvard.edu

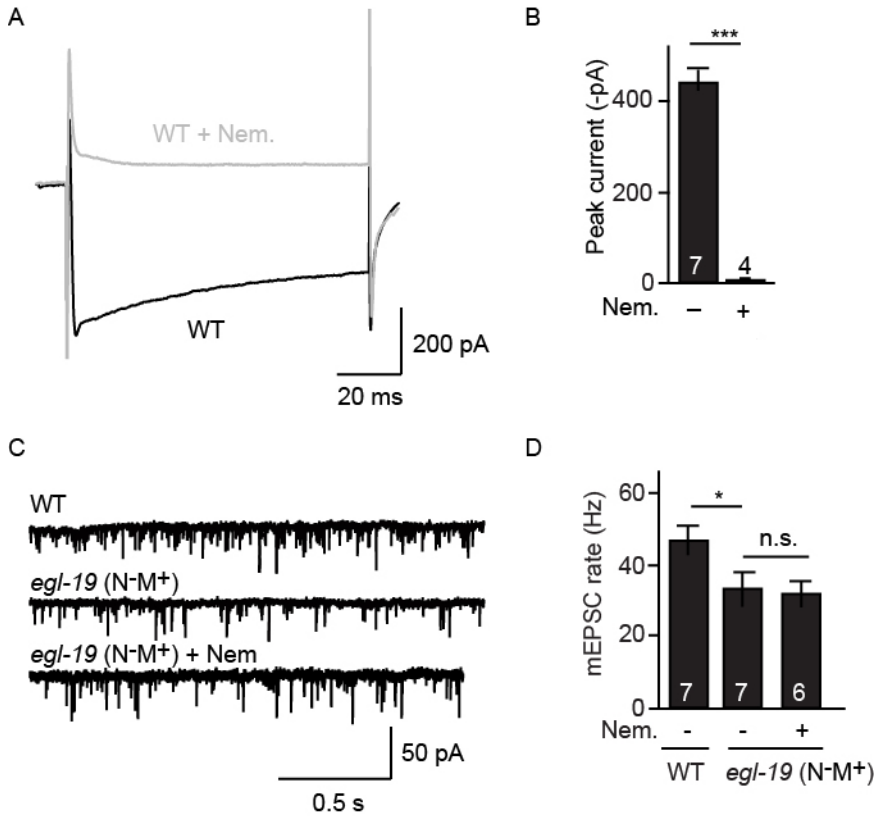

Figure S1. Tong et al.

Figure S1. Supplementary data related to Figure 1. (A-B) Nemadipine effectively blocked the EGL-19/CaV1 current in adult body muscles. Voltage-activated Ca^{2+} currents were recorded from adult body wall muscles of wild type adults with and without addition of 10 μM Nemadipine to the bath solution. Currents were recorded at holding potentials of -60 to +40 mV. Averaged traces (A) and mean current amplitude (B) at +10 mV are shown. (C-D) Nemadapine effects on mEPSC rate are mediated by inhibiting EGL-19/CaV1 channels expressed in neurons. Tonic ACh release was recorded from adult *egl-19* null mutants containing a transgene that expresses EGL-19 in muscles, designated *egl-19* (N^-M^+) animals. The mEPSC rate in was significantly lower than in wild type controls and was not further reduced by Nemadapine treatment. The number of animals analyzed is indicated for each genotype. Values that differ significantly are indicated (***, p <0.001; *, p <0.05; n.s., not significant). Error bars indicate SEM.

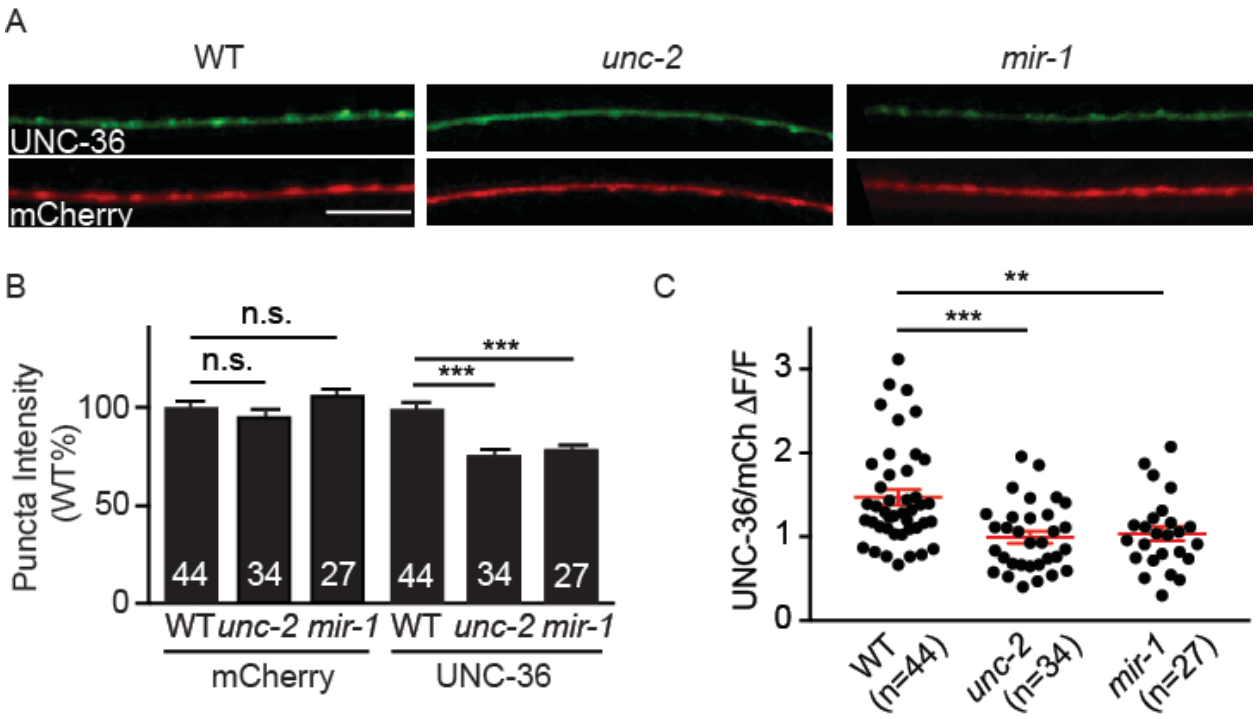

Figure S2. Tong et al.

Figure S2. Supplementary data related to Figure 2. The distribution of co-expressed mngUNC-36 and mCherry in the dorsal cord axons of DA/DB neurons are compared. Representative images (A), mean puncta intensity (B), and mean mngUNC-36 puncta ΔF/F (normalized to mCherry) (C) are shown. mngUNC-36 puncta intensity and synaptic accumulation (ΔF/F) in DNC axons was significantly decreased in *unc-2* and *mir-1* mutants. By contrast, mCherry puncta intensity was unaltered in both mutants. Values that differ significantly are indicated (***, p <0.001; **, p <0.01; n.s., not significant). The number of animals analyzed is indicated for each genotype. Error bars indicate SEM. Scale bar indicates 10 μm.

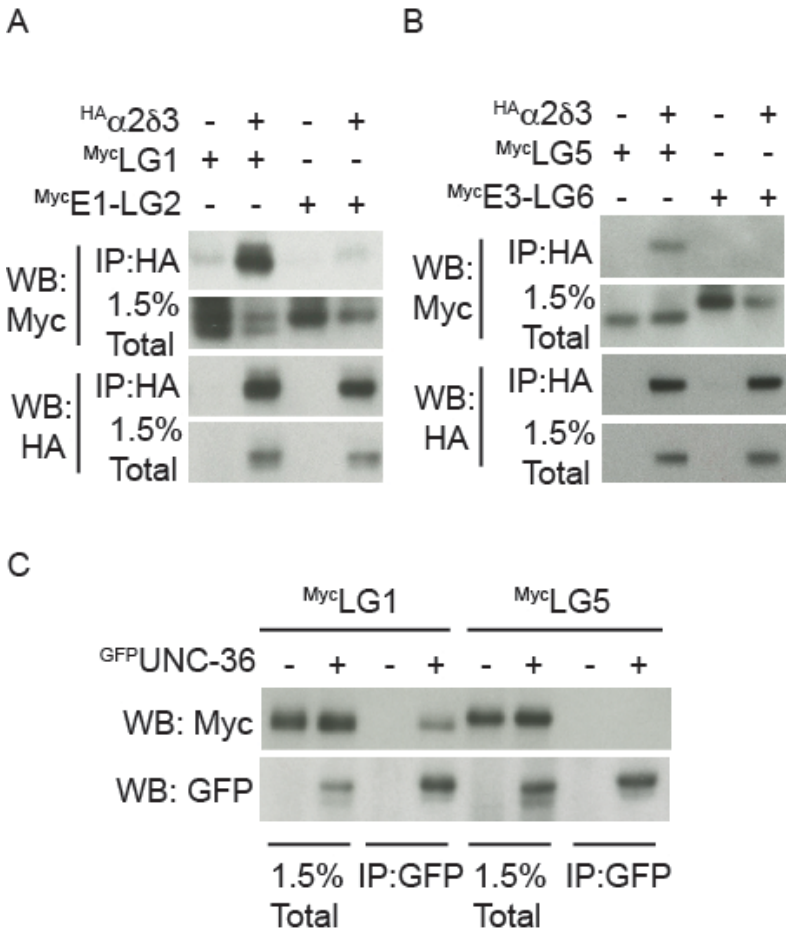

Figure S3. Tong et al.

Figure S3. Supplementary data related to Figure 5. α-NX domains required for co-immunopreciptation with α2δ were mapped using mammalian (A-B) and *C. elegans* (C) proteins. For mouse NX-1α, the isolated LG1 (A) and LG5 (B) domains co-immunoprecipitated with α2δ-3, whereas the isolated LG2 and LG6 domains failed to co-immunoprecipitate with α2δ-3. For the *C. elegans* proteins, the isolated LG1 domain co-immunoprecipitated with UNC-36, while the isolated LG5 domain did not (C). Proteins carrying the indicated epitope tags were expressed in transfected HEK cells and detected by immunoprecipitation and western blotting.

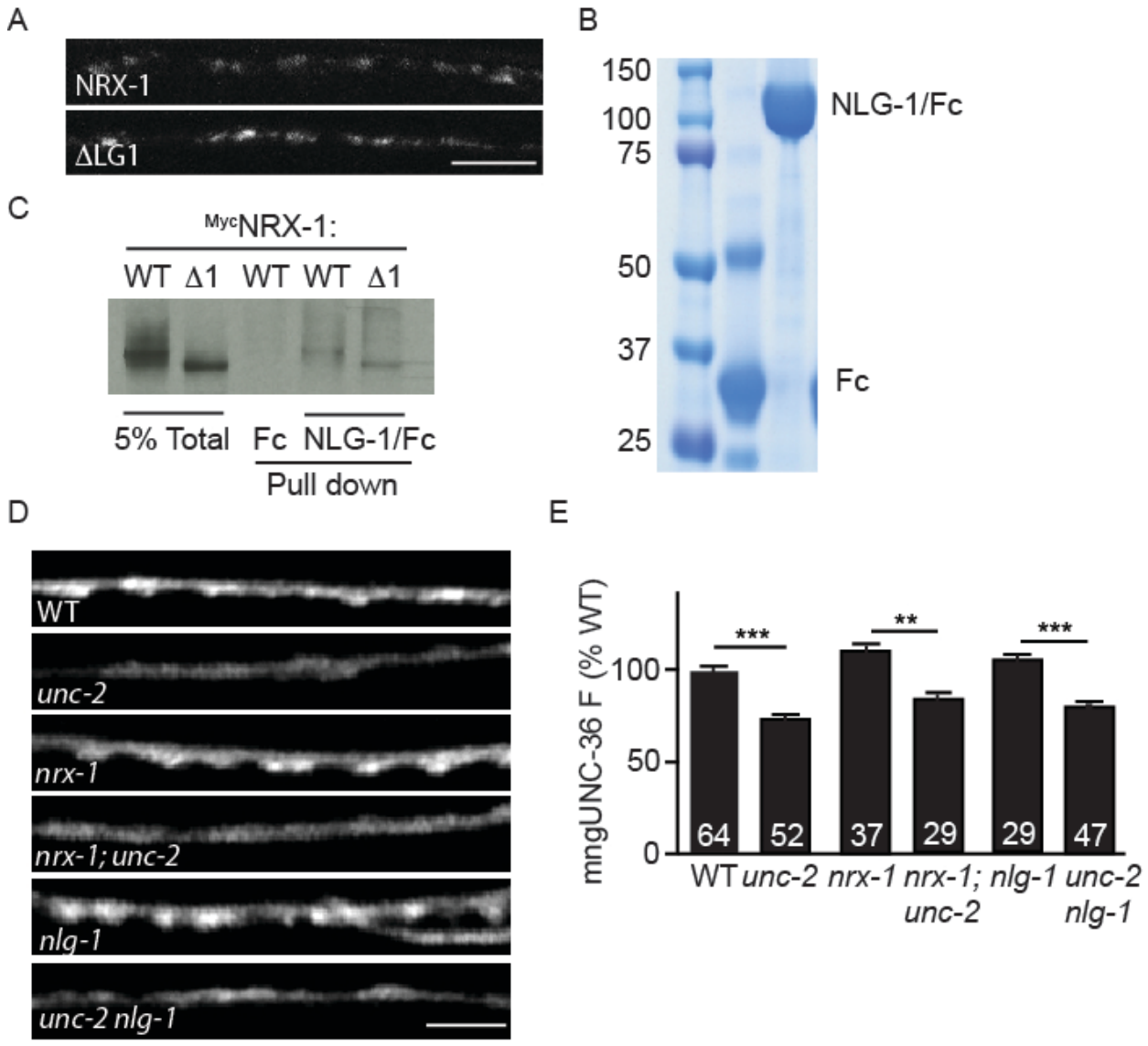

Figure S4. Tong et al.

Figure S4. Supplementary data related to Figure 7. (A-C) Deleting the LG1 domain did not prevent trafficking of NRX-1 to the dorsal nerve cord (A) nor did it prevent binding to NLG-1 (C). Representative images (A), a coomassie stained gel documenting expression of the Ig Fc domain, and the NLG-1 ectodomain fused to Fc (NLG-1/Fc) expressed in HEK cells (B), and pull down of Myc-tagged NRX-1 and ΔLG1 with Fc and NLG-1/Fc (C) are shown. (D-E) mngUNC-36 puncta intensity in DNC axons was significantly decreased in *unc-2* mutants and this effect was not reversed by mutations inactivating NRX-1 nor those inactivating NLG-1. Representative images (D) and mean puncta intensity (E) are shown for each genotype. Values that differ significantly from wild type controls are indicated (***, p <0.001; **, p <0.01). The number of animals analyzed is indicated for each genotype. Error bars indicate SEM. Scale bar indicates 10 μm.

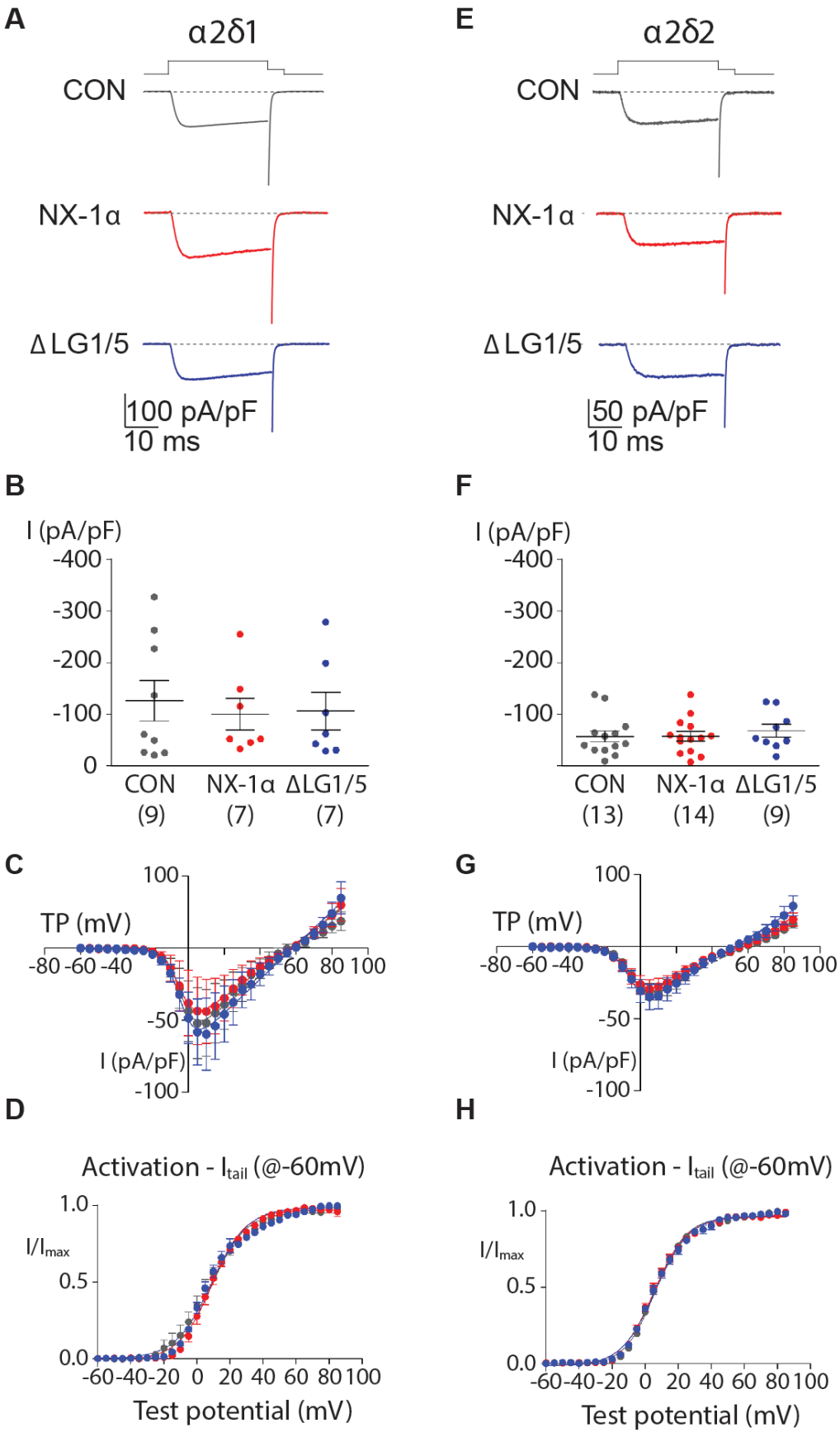
A
α2δ1
CON
NX-1α
ΔLG1/5
100 pA/pF
10 ms
E
α2δ2
CON
NX-1α
ΔLG1/5
50 pA/pF
10 ms
B
I (pA/pF)
-400
-300
-200
-100
0
CON (9)
NX-1α (7)
ΔLG1/5 (7)
F
I (pA/pF)
-400
-300
-200
-100
CON (13)
NX-1α (14)
ΔLG1/5 (9)
C
TP (mV)
100
-80 -60 -40
60 80 100
-50
I (pA/pF)
-100
G
TP (mV)
100
-80 -60 -40
60 80 100
-50
I (pA/pF)
-100
D
Activation - I_tail (@-60mV)
I/I_max
1.0
0.5
0.0
-60-40-20 0 20 40 60 80 100
Test potential (mV)
H
Activation - I_tail (@-60mV)
I/I_max
1.0
0.5
0.0
-60-40-20 0 20 40 60 80 100
Test potential (mV)

Figure S5. Supplementary data related to Figure 8. NX-1α has no effect on CaV2.2 channels containing α2δ-1 or α2δ-2. Properties of whole cell CaV2.2 currents recorded from tsA201 cells expressing CaV2.2, CaVβ_3 and α2δ-1 (A-D) or α2δ-2 (E-H) subunits, co-transfected with empty pcDNA3.1 vector (CON), mouse NX-1α (NX-1α), or mutant NX-1α lacking LG1 and LG5 (ΔLG1/5). All recordings were performed using 1 mM calcium as the charge carrier and the identity of the co-transfected construct was unknown by the experimenter at the time of recording. The experimenter was unblinded after the analysis.

(A,E) Individual whole cell CaV2.2 current recordings from six different tsA201 cells expressing CaV2.2, CaVβ_3, and CaVα2δ-1 (A) or CaVα2δ-2 (E) co-transfected with the indicated plasmids. Currents were evoked by 30 ms step depolarization to +10 mV from a holding potential of -100 mV, and tail currents were captured during a 5 ms repolarizing step to -60 mV.

(B,F) Peak CaV2.2 current densities, evoked by step depolarization to +10 mV from holding potential of -100 mV, from each cell co-transfected with the indicated constructs. Each point represents measurement from one cell. Mean and SEM are shown for each condition. The number of cells in each data set is shown in parenthesis below each condition. Shapiro-Wilk normality tests: α2δ-1/CON, p = 0.06; α2δ-1/NX-1α, p = 0.07; α2δ-1/ ΔLG1/5, p = 0.07; α2δ-2/CON, p = 0.04; α2δ-2/NX-1α, p = 0.50; α2δ-2/ΔLG1/5, p = 0.35. Consequently, we used non-parametric Kruskal-Wallis tests and found no significant differences across conditions: p = 0.9798 for α2δ-1 and p = 0.7884 for α2δ-2.

(C,G) Average peak CaV2.2 current voltage (I-V) relationships measured in cells expressing CaV2.2, CaVβ_3, and α2δ-1 (C) co-transfected with CON (n = 7), NX-1α (n = 5) and ΔLG1/5 (n = 7) or those expressing α2δ-2 (G) co-transfected with CON (n = 10), NX-1α (n = 9) and ΔLG1/5 (n = 6). Currents were evoked by depolarizing steps of increasing amplitudes in 5 mV intervals from a holding potential of −100 mV. Boltzmann-linear functions were fit to individual data sets from each cell and used to estimate activation mid-point ($V_{1/2}$), slope factor (k) and reversal potential (V_{rev}) in Table 1.

(D,H) Activation curves generated from peak tail $Ca_V2.2$ current amplitudes captured at -60 mV plotted against the value of the preceding test depolarization in cells expressing α2δ-1 (D) co-transfected with CON (n = 5), NX-1α (n = 5) and ΔLG1/5 (n = 7), or those expressing α2δ-2 (H) co-transfected with CON (n = 10), NX-1α (n = 9) and ΔLG1/5 (n = 5). Voltage steps were applied every 10 sec, in 5 mV increments, between -60 and +85 mV. I/Imax was measured for tail currents over the range of test potentials. Boltzmann functions were fit to data from each cell and average $V_{1/2}$ and k values estimated and documented in Table 1. CaV2.2 activation curves were not significantly different across the conditions.

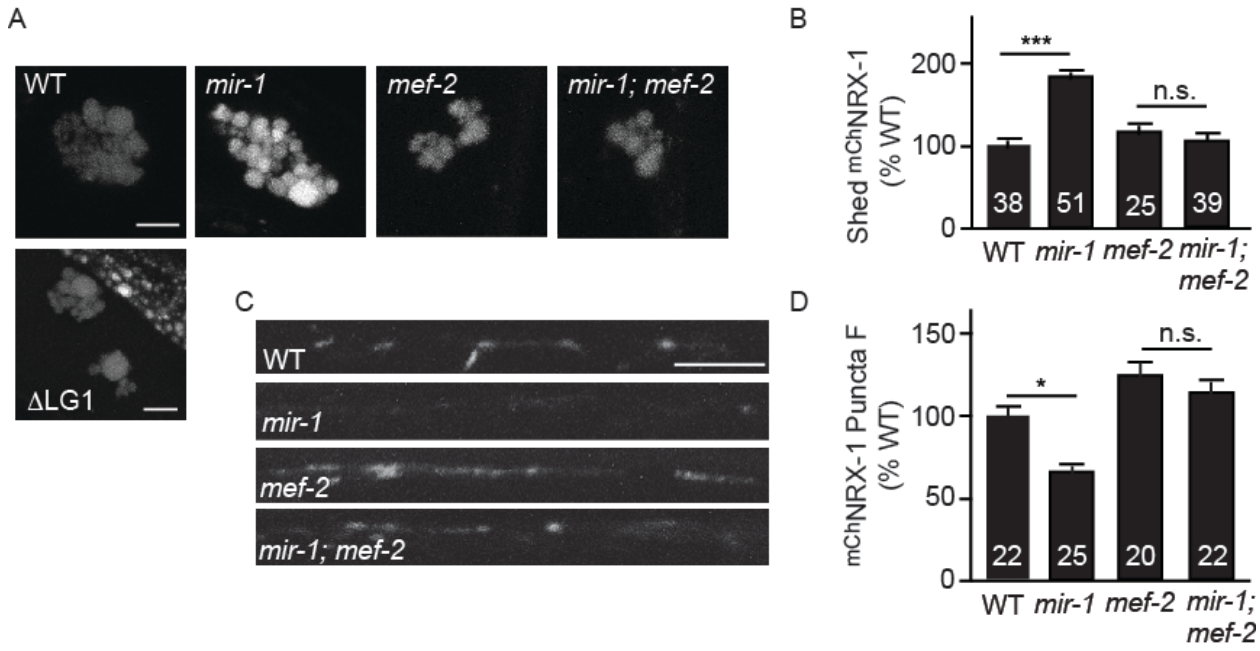

Figure S6. Tong et al.

Figure S6. Supplementary data related to Figure 9. Increased shedding of ^{mCh}NRX-1 in *mir-1* mutants was blocked by mutations inactivating MEF-2. Shed ^{mCh}NRX-1 was assayed by analyzing coelomocyte fluorescence (A-B). Uncleaved ^{mCh}NRX-1 was assayed by analyzing dorsal cord puncta fluorescence (C-D). Deleting the LG1 domain did not prevent ^{mCh}NRX-1 shedding (A). Representative images (A,C), mean coelomocyte fluorescence (B), and mean puncta fluorescence (D) are shown. Values that differ significantly from wild type controls are indicated (***, p <0.001; *, p <0.05; n.s., not significant). The number of animals analyzed is indicated for each genotype. Error bars indicate SEM. Scale bar indicates 10 μm.

	Con mean ± se (N)	NX-1α mean ± se (N)	ΔLG1/5 mean ± se (N)
α2δ1			
V_{rev} (mV)	54.20 ± 3.62 (6)	55.70 ± 2,03 (5)	52.08 ± 2.50 (7)
V_{50} (mV)	-3.05 ± 0.89 (6)	-1.78 ± 1.77 (5)	-4.40 ± 0.51 (7)
k (mV)	4.47 ± 0.42 (6)	4.55 ± 0.29 (5)	4.50 ± 0.22 (7)
V_{50} (mV)	5.68 ± 3.71 (5)	8.70 ± 2.21 (5)	7.16 ± 1.42 (7)
k (mV)	11.45 ± 1.17 (5)	8.97 ± 0.46 (5)	10.18 ± 0.86 (7)
α2δ2			
V_{rev} (mV)	57.77 ± 0.52 (10)	55.10 ± 1.90 (10)	54.62 ± 2.96 (6)
V_{50} (mV)	-5.95 ± 0.53 (10)	-4.64 ± 1.42 (10)	-4.77 ± 1.44 (6)
k (mV)	4.20 ± 0.09 (10)	5.22 ± 0.52 (10)	5.34 ± 0.48 (6)
V_{50} (mV)	6.51 ± 0.36 (10)	5.59 ± 1.20 (9)	5.08 ± 1.33 (7)
k (mV)	9.49 ± 0.36 (10)	9.78 ± 0.36 (9)	9.81 ± 0.58 (7)
α2δ3			
V_{rev} (mV)	54.02 ± 1.61 (17)	51.92 ± 2.63 (9)	52.75 ± 1.33 (12)
V_{50} (mV)	-5.87 ± 0.62 (17)	-5.70 ± 0.77 (9)	-5.39 ± 0.44 (12)
k (mV)	4.84 ± 0.32 (17)	4.40 ± 0.30 (9)	4.84 ± 0.27 (12)
V_{50} (mV)	6.54 ± 0.85 (14)	4.22 ± 0.99 (8)	4.78 ± 0.63 (10)
k (mV)	10.19 ± 0.34 (14)	10.33 ± 0.69 (8)	10.14 ± 0.25 (10)

Table S1. Supplementary data associated with Figure 8.

NX-1α does not affect biophysical properties of CaV2.2 currents co-expressed with CaVα2δ-1, CaVα2δ-2 or CaVα2δ-3. Summary of properties of CaV2.2 channel currents recorded from tsA201 cells expressing CaV2.2 and $CaV\beta_3$ together with one of $CaV\alpha_2\delta$-1, $CaV\alpha_2\delta$-2 or $CaV\alpha_2\delta$-3 subunits, and with one of empty pcDNA3.1 vector (CON), neurexin protein (NX-1α) or mutant NX-1α lacking LG1 and 5 (ΔLG1/5). All recordings were performed using 1 mM calcium as the charge carrier. Experiments were carried out with the experimenter blinded to the experimental conditions (CON, NX-1α, ΔLG1/5). The experimental conditions were only revealed after analyses were completed. Boltzmann-linear functions were fit to each individual CaV2.2 current voltage (I-V) relationships and activation mid-point ($V_{1/2}$), slope factor (k) and reversal potential (Vrev) values were estimated (upper set of values in each panel). We also fit Boltzmann functions for CaV2.2 activation curves from each cell, by measuring tail current amplitudes at -60 mV that were preceded by a series of test pulses. $V_{1/2}$ and k values are shown from these fits (lower set of values in each panel). Values shown are averages ± SE, (N). N represents the number of cells.